The Spitak (Armenia) earthquake of 7 December 1988: field observations, seismology and tectonics

A. Cisternas*, H. Philip†, J. C. Bousquet†, M. Cara*, A. Deschamps‡, L. Dorbath*§, C. Dorbath*§, H. Haessler*, E. Jimenez*, A. Nercessian‡, L. Rivera*, B. Romanowicz‡, A. Gvishiani‖, N. V. Shebalin‖, I. Aptekman‖, S. Arefiev‖, B. A. Borisov‖, A. Gorshkov‖, V. Graizer‖, A. Lander‖, K. Pletnev‖, A. I. Rogozhin‖ & R. Tatevossian‖

* Institut de Physique du Globe, Université Louis Pasteur, 5 rue René Descartes, 67084 Strasbourg, Cedex, France
† Laboratoire de Géologie Structurale, Université des Sciences et Techniques du Languedoc, Place E. Bataillon, 34060 Montpellier, France
‡ Institut de Physique du Globe, Université Pierre et Marie Curie, 4 place Jussieu, 75230 Paris Cedex 05, France
§ Institut Français de Recherche Scientifique pour le Développement en Coopération, ORSTOM, 213 rue La Fayette, 75480 Paris Cedex 10, France
‖ Institute of Physics of the Earth, 10 Bolshaya Gruzinskaya, 123810 Moscow, USSR

The epicentre of the destructive earthquake that devastated northern Armenia, the strongest in the region since historical times, is located within the Lesser Caucasus, a mountain country subjected to north–south compression by the push of the Arabian plate. A French–Soviet field expedition studied surface breaks and aftershock activity. The fault scarp could be followed for 13 kilometres and showed a reverse dislocation of 1.6 metres. Aftershocks are shallower than 13 kilometres, and delimit a ruptured surface of about 300 km^2.

A DESTRUCTIVE earthquake devastated the region around the cities of Spitak, Leninakan and Kirovakan in northern Soviet Armenia on December 7, 1988, at 07:41 UT (latitude 40.94° N, longitude 44.29° E, depth 10 km according to the US National Earthquake Information Center (NEIC); 41.15° N, 44.25° E after the Euro-Mediterranean Seismological Centre; 40.84° N, 44.32° E, depth 10 km using 19 local Soviet stations). Its magnitude was 7.0 according to the Seismological Centre of Obninsk[1], 6.9 according to NEIC and 6.7 according to the Institut de Physique du Globe de Strasbourg. This was the largest earthquake in this region since historical times. Official figures give 25,000 people dead, the city of Spitak being destroyed to 90%, Leninakan to 50% and Kirovakan to 20%. The maximum intensity, $I_0 = X$ in the MKS scale, was observed in the region to the north-west of Spitak.

A French–Soviet team formed by seismologists and geologists went to the source region 10 days after the main shock in order to register aftershock activity and to map the surface breaks (Soviet seismologists and geologists arrived at the epicentral zone on 10 December). A similar American group from the US Geological Survey[2] also worked in the area.

Geodynamics

The epicentral zone is located within the Lesser Caucasus, which is dominated by a north–south compressive tectonics resulting from the young continental collision between the Arabian plate and the Russian Platform[3]. The rate of convergence has been evaluated at 3 cm yr^{-1}. Figure 1 illustrates the main features of this collision; there is lateral ejection of the Turkish block to the west along the North Anatolian Fault, the Iranian block to the east, and the squeezing of a region about 800 km wide between the northern front of the Arabian wedge and the Russian Platform.

The Lesser and Great Caucasus are located to the north of this region. Caucasian tectonics is characterized by reverse faulting and folding associated with large strike-slip faulting. Present and neogene tectonics of northern Armenia shows that north–south compression coexists with east–west extension related to recent volcanism along north–south-oriented normal faulting, and with the Borjomi–Kasbeg left-lateral strike-slip fault[3].

The earthquake fault belongs to the approximately east-west Sevan–Akera deep thrust zone, the old Tethys suture, which borders the Lesser Caucasus to the south, running along the northern border of the Sevan Lake and to the north of the Aragat volcano and volcanic plateau. The Pambak river runs along the fault zone, the structural disposition of its basins suggesting a right-lateral component of the motion across the fault.

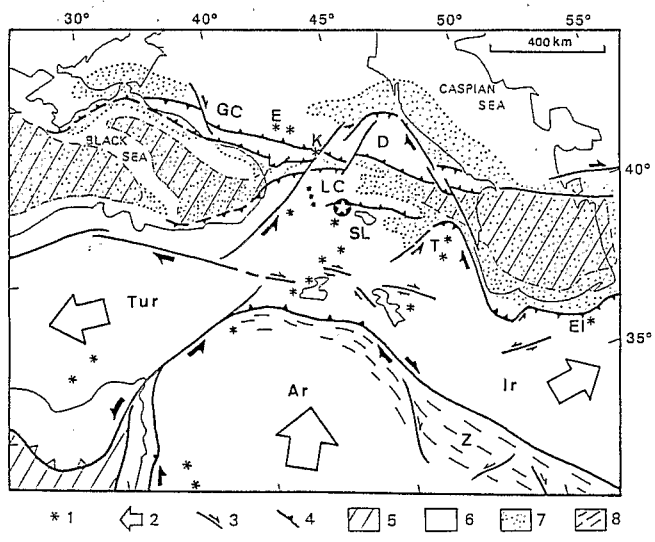

FIG. 1 Present-day tectonic features characterizing the Caucasus. The star shows the epicentre of the 7 December 1988 Armenian earthquake. 1, Recent volcanoes; the Aragat volcano is just below the epicentre. 2, Relative motion with respect to Eurasia. 3, Major strike-slip faults. The north-east-oriented Borjomi–Kasbeg fault passes next to the Kasbeg volcano. 4, Major thrusts; the Sevan–Akera fault zone passes by the epicentre of the Spitak earthquake. 5, Oceanic or intermediate crust. 6, Continental crust. 7, Main sedimentary basins. 8, Recent folding at the border of the Arabian plate. GC, Great Caucasus; D, Dagestan; LC, Lesser Caucasus; T, Talesh; El, Elbros; Ir, Iranian block; Tur, Turkish block; Ar, Arabian plate; Z, Zagros; SL, Sevan Lake; K, Kasbeg volcano; E, Elbruz volcano.

The main shock

The main shock was preceded by a foreshock of magnitude $M_L = 3$, on 6 December at 15:27, and was followed 4 min 20 s later by a large aftershock of magnitude $M_L = 5.8$ (ref. 1). Different focal mechanisms have been calculated by different groups, the first being obtained by the analysis of surface waves. Two days after the earthquake, a mechanism (Fig. 2*a*) was obtained[4] using Love and Rayleigh waves at periods ranging from 20 to 50 s (ref. 5). This result (azimuth = 309°, dip = 29° for the fault and slip vector = 107°) was conveyed to NEIC in Golden, Colorado, and to the Institute of Physics of the Earth in Moscow. The thrust component was shown clearly on this first solution, although there was no resolution of the horizontal component of the slip, and the half-depth of the source was found to be 7 km. A week later, the global Geoscope[6] network permitted a more constrained mechanism[7] to be obtained by using Rayleigh waves retrieved by dial-up teletransmission from eight stations at a longer period ($180 < T < 320$ s) and at a fixed depth of 10 km. Figure 2*b* shows this solution, which is remarkably close to what was observed in the field (azimuth = 299°, dip = 72° for the fault and slip vector = 135°). The residuals for the amplitude at different azimuths were small, and the phase was well explained except at those azimuths where rapid variations occur. The seismic moment was 1.6×10^{26} dyne cm for the single-station Strasbourg solution, and 2×10^{26} dyne cm for the Geoscope determination. With these values, the expected length of the fault should be of the order of 20 km if we estimate a mean slip of 2 m and a fault width of 15 km from field observations. Broad-band body-wave modelling, obtained four months later when the records became available, is shown in Fig. 2*c* (azimuth = 30°, dip = 60° for the fault plane and slip vector = 110°). The P and SH waves from broad-band and long-period stations, low-pass-filtered at 6 s, are well explained by two pulses, each with a duration of 3 s and a seismic moment of $\sim 0.4 \times 10^{26}$ dyne cm, separated in time by 12–16 s. A small precursor is needed to fit the beginning of the signal. Separation between the pulses is larger in the Chinese stations than in the African, European and American ones, suggesting that the rupture propagated from east to west.

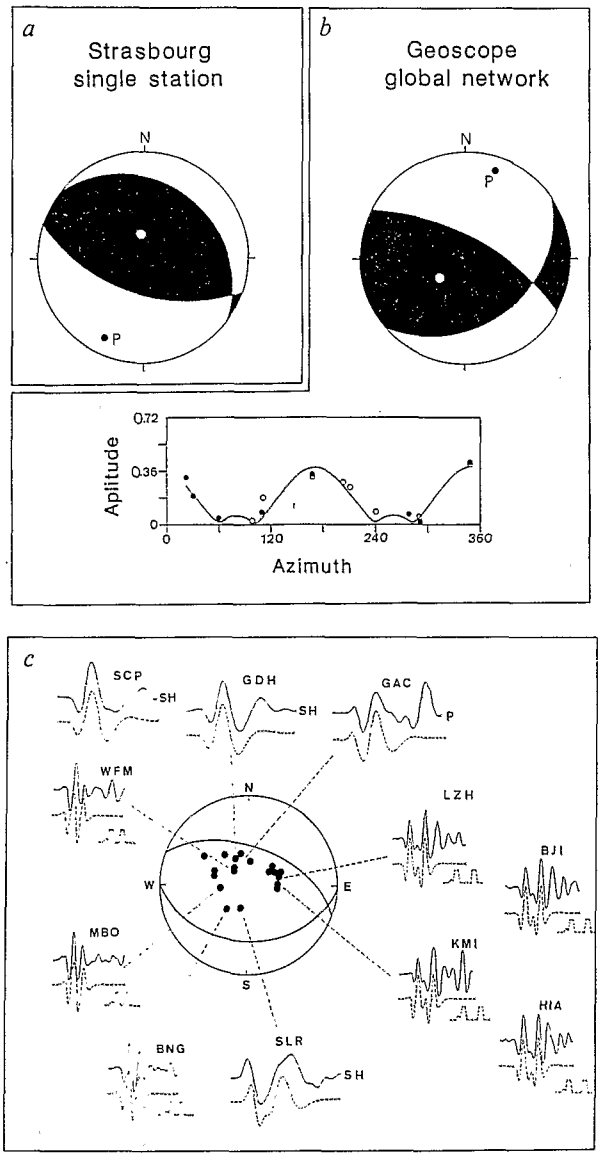

FIG. 2 Focal-mechanism solutions for the main shock. The circles represent the horizontal projection of the lower hemisphere of a sphere centred at the source. The fault plane and a plane orthogonal to the slip are shown. Dark areas are regions in which the source pushes towards the station. *a*, Strasbourg solution from analysis of surface waves of the Echery broad-band records 48 h after the earthquake. *b*, Solution obtained one week later from Rayleigh-wave data from 8 globally distributed Geoscope long-period stations. Lower figure show the fit of amplitude as a function of the azimuth at the source. *c*, Broad-band body waves and long-period P and SH waves from the GDSN and Geoscope network. Solid lines are recorded seismograms, and segmented lines are theoretical. The model consists of two pulses, 3 s wide, separated by 12 (MBO and BNG) to 16 s (Chinese stations LZH, BJI, KMI and HIA), preceded by a small precursor.

Besides the tectonic evidence, we observed that focal mechanisms in the Caucasian region, those calculated by Jackson and McKenzie[8] for example, are compatible with a north–south compression. The mechanism of the Spitak earthquake thus gives new, high-quality additional information to confirm the general features of the tectonics of the region.

Surface breaks

Surface breaks oriented roughly 120° N have been observed between the town of Spitak and the village of Gekhasar (Fig. 3). They show a reverse faulting dipping to the north with a right-lateral offset. The overall situation is rather simple in comparison with other well documented reverse-faulting earthquakes, such as El Asnam[9] or Tabas[10].

The surface breaks present a narrow band of pressure ridges within the soil cover and alluvians (Fig. 4*a*), whereas a neat scarp is observed within the bedrock (Fig. 4*b*). The fault plane dips to the north at an angle of between 50° and 80°. Striations on fault faces are consistent with reverse motion with a slight right-lateral component when the azimuth is 120° N, and with pure reverse motion when the strike is east–west. Vertical and horizontal displacements increase from north-west to south-east. We observed 40 cm of vertical displacement and 15 cm of right-lateral offset near Gekhasar, but 160 cm of vertical displacement and 40 cm of right-lateral displacement near Spitak. Shortening of about 70 cm was measured across an irrigation duct at about 1 km to the east of Gekhasar. Some secondary features near Gekhasar consist of normal faulting within the thrusting block resulting from the collapse of the hanging compartment.

We have mentioned that the seismic-moment calculation pointed to a rupture surface of ~ 300 km^2. Then, if the aftershocks are shallower than 15 km, the fault length should be at least 20 km, which is greater than what is observed at the surface. This discrepancy must be explained. No continuation of the fault breaks have been found east of Spitak up to now. On the other hand, a 200-m break effects an anticline hinge about 5 km west-northwest of Gekhasar (Fig. 3). It is possible that the broken area appears only partially at the surface, but also that brittle rupture is replaced by continuous plastic deformation. If the fold is the surface expression of the blind thrust existing at depth, then the total length of the thrust becomes 16 km, in better agreement with the estimations of seismic moment.

The observed fault separates different geological formations at most places (Palaeocene volcanic rocks in the northern block,

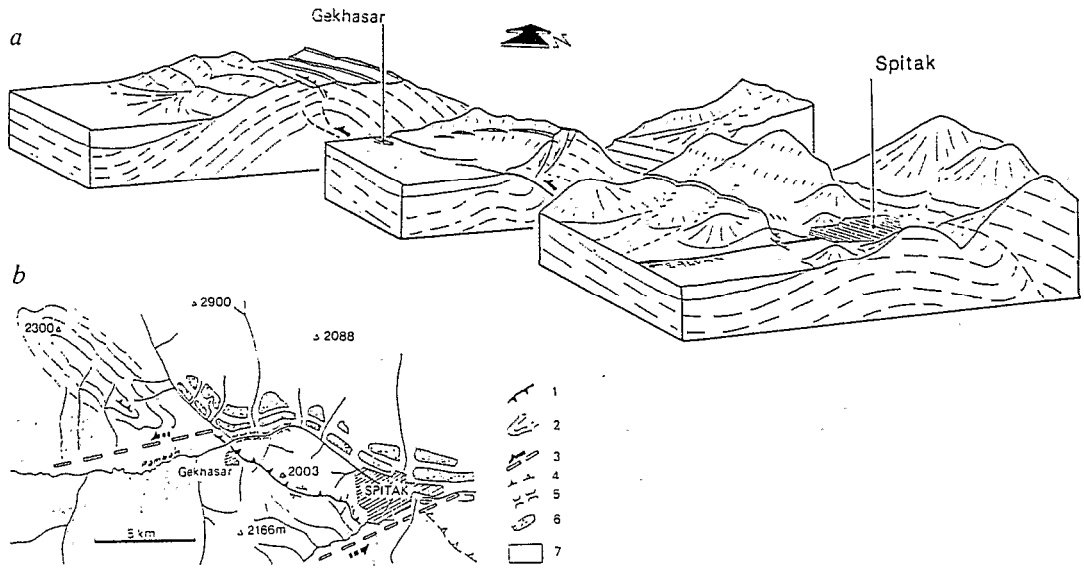

FIG. 3 Surface breaks and deformation related to the main shock. *a*, Block diagram showing surface ruptures between Spitak and Gekhasar and the fold to the west of Gekhasar. A geological fault exists to the east of Spitak but was not activated during the earthquake. *b*, Same as *a* but on the horizontal plane. High points are indicated, along with their elevation in metres. 1, Thrusts activated during the earthquake. 2, Layering within the anticline west-northwest of Gekhasar. 3, Inferred left-lateral strike-slip faults offsetting the segments of the thrust. 4, Thrusts not activated during the main shock. 5, Pambak river gorge. 6, Uplifted Quaternary terraces. 7, Quaternary sedimentary filling in subsiding valleys.

and upper Cretaceous limestones to the south). Therefore it is likely that the fault acted as a normal fault in the past, and that the motion later changed to reverse. The limestones are distorted and folded against the fault gauge at the contact, in agreement with the recent sense of motion (Fig. 3). There is no geomorphological evidence for a fault scarp along this geological contact. Nevertheless this fault has been an active thrust during Quaternary times, as indicated by the exposures along the road from Spitak to Leninakan, near Gekhasar. In fact, Quaternary volcanic tuffs and alluvial deposits are faulted and tilted near the fault trace. A further and more striking piece of evidence is the overall disposition of fluvial deposits on both sides of the fault. To the north of the fault trace, or its continuation, there is a system of well developed successive terraces that have been elevated and then eroded by the Pambak river and tributaries. On the other hand, south of the fault trace, the valleys are smoothly filled with sediments, swamps are present and no terraces are observed. This disposition indicates that during Quaternary times the southern compartment of the fault subsided but the northern one was uplifted. As this earthquake is the largest observed during historical times, it is certain that no conclusions regarding seismic hazard may be obtained from the historical record alone. It is then necessary to appeal to palaeoseismic studies to estimate maximum possible earthquake and recurrence times.

Aftershocks

A seismic network of 25 portable stations and 3 accelerometers was arrayed around the source region by the French team 10 days after the main shock (Fig. 5). The network, with a diameter of about 50 km, consisted of 10 MEQ analog recorders with L4C Mark Product seismometers, six Geostras digital three-component autonomous stations recording on magnetic tape, and a portable digital telemetric network, built in Strasbourg, with one three-component and eight vertical-component stations centred at Spitak.

Day-to-day location of the aftershocks was routinely performed during the field experiment together with magnitude determination and observation of other parameters of the seismic regime. In Fig. 5 we show the distribution of 259 well recorded aftershocks corresponding to the period from 22 December 1988 to 1 January 1989. The relative disposition of the events with respect to the surface deformations and breaks indicates that most of the activity is concentrated to the north of the surface scarps. The aftershock cloud is elongated along the trend of the fault. One notable feature is the very low level of activity

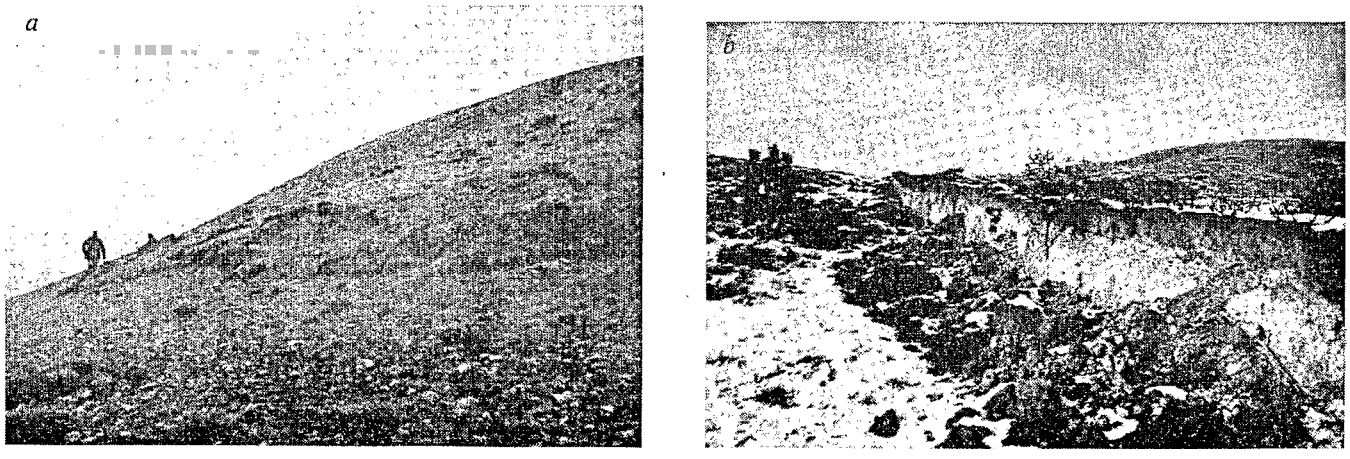

FIG. 4 Representative surface breaks looking towards the west. *a*, Pressure ridges on soil. Extension cracks indicate a right-lateral component of slip. *b*, Scarp in volcanic rock showing 1.6 m of reverse vertical offset. Bushes were burnt next to the fault trace, possibly because of escape and ignition of gases through tension cracks.

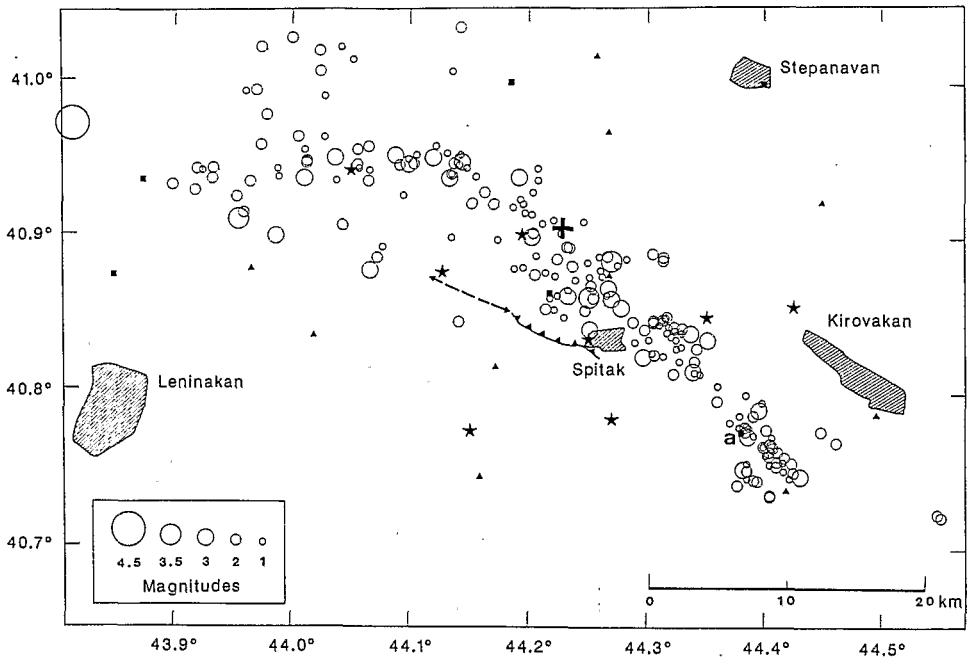

FIG. 5 Space distribution of aftershocks within the period from 22 December 1988 to 1 January 1989. The seismic network is composed of eight telemetric digital stations centred at Spitak (stars), six Geostras three-component digital stations (squares) and ten analog Sprengnether MEQ stations (triangles). The epicentre of the main shock, localized relative to the 31 December aftershock, is shown as a black cross. The fault trace, the fold axis (dashed line) and the cities of Spitak, Leninakan, Kirovakan and Stepanavan are shown for reference. **a**, denotes the Aidarli station.

in the vicinity of the rupture zone or its estimated extension to the west into the fold. Aftershocks concentrate on the border of this gap. It is reasonable to assume that this surface corresponds to the zone of rupture during the main shock. The area of surface involved is ~300 km^2, in agreement with the estimations from the seismic moment. Further clustering is observed in the neighbourhood of Spitak and also to the east near Aidarli. These clusters are separated by a gap that may correspond to one of the strong aftershocks. Most of the aftershocks are shallower than 13 km (Fig. 6*a*). A cross-section orthogonal to the fault trace shows that there is a concentration of aftershocks near a plane dipping 50° to the north (Fig. 6*b*).

Discussion

The fault of Spitak is simpler than that of Al Asnam[9] and has produced few secondary features. Nevertheless, it is segmented and we find that at least two segments moved during the main shock. One corresponds to the fault breaks between Spitak and Gekhasar, and the other to the blind thrust to the west of Gekhasar. The almost total destruction of Spitak is certainly related to the fact that the trace of the fault passed along the border of the town. A third segment, to the east of Spitak, is clearly recognized on the field as the continuation of the Spitak fault, but showed no evidence of surface rupture in spite of the cluster of aftershock activity that may be associated with it. It is likely that these segments are offset and separated by left-lateral strike-slip faults (one at least being evident on a SPOT satellite image) trending 80° N and forming a tectonic system that is kinematically consistent with a north–south compression (Fig. 3*b*). This scheme is substantiated by the drainage network, which follows the fault system. The sense of propagation of the rupture will be discussed in detail elsewhere; as the main shock has a relative location close to the end of the fault, near Spitak (Fig. 5), we conclude that the rupture propagated from east to west. The largest aftershock, 4 min 20 s after the main shock, is located to the east of Spitak, and may thus explain the gap and clusters near Aidarli.

The occurrence of the Spitak earthquake draws attention to the problem of determining the maximum possible earthquake in the region. This is the strongest earthquake in northern Armenia since historical times[11]. Spitak was affected by an earthquake of magnitude 5 in 1967, Kirovakan suffered a shock

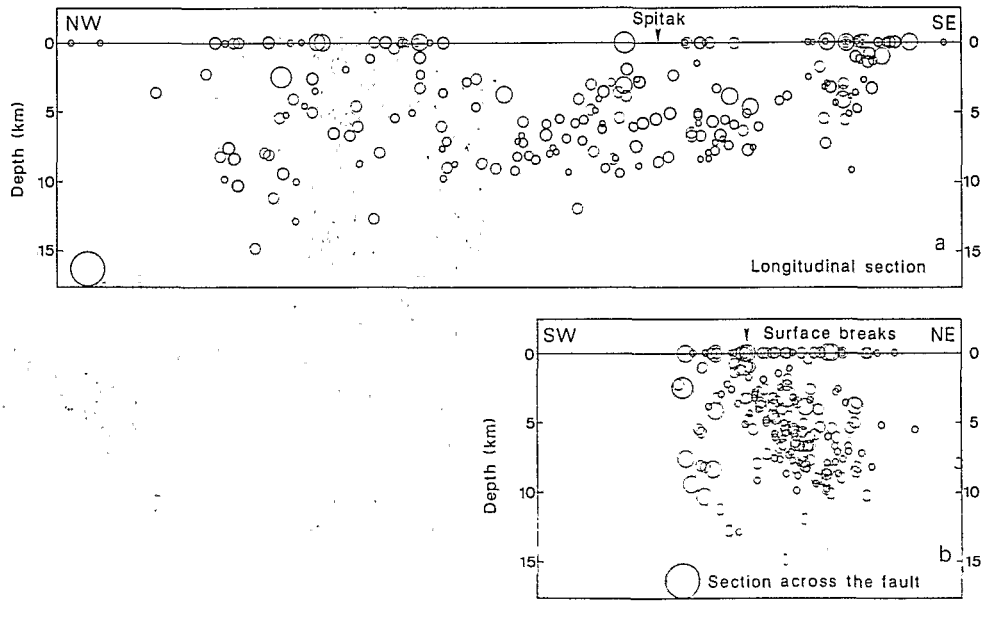

FIG. 6 Vertical distribution of aftershock activity. *a*, Section along the fault trace. Hypocentres are not deeper than 13 km. *b*, Section across the fault scarp. The geometry suggests a fault plane dipping about 50° to the north. Note that some shocks have an automatically fixed zero depth.

of magnitude 5.3 in 1911 and Leninakan was the site of an earthquake of magnitude 5.7 in 1926. Few seismologists believed that an earthquake as severe as that of 7 December 1988 was possible in this region. It is clear that seismic history alone is not sufficient to arrive at such conclusions. One way to improve the assessment of seismic hazard in this region, where continental collision is dominant and seismicity is confined to the crust, is to increase the knowledge of active faulting, for example by improvement of the permanent seismic network, neotectonic mapping of Quaternary deformation, analysis of aerial and satellite images, and the use of palaeoseismology in appropriate sites to give an insight into past activity.

Pattern-recognition analysis of earthquake-prone areas made by the Soviet group for events of magnitude $M > 6.5$ in Armenia classified as dangerous an object around Leninakan that included the epicentre of the 7 December Spitak earthquake[12]. Further study[13] established an object close to Erevan as being dangerous for earthquakes of magnitude $M > 7$. It is now recommended that this latter region also be subjected to short-term prediction studies, because a nuclear power plant is operational there. □

Received 6 March; accepted 31 May 1989.

1. Shebalin, N. V. & Borisov, B. A. *Priroda* (in the press).
2. Maggs, W. W. *Eos* **70**, 17 (1989).
3. Philip, H., Cisternas, A., Gvishiani, A. & Gorshkov, A. *Tectonophysics* **161**, 1–21 (1989).
4. Ekström, G., Dziewonski, A. & Steim, J. M. *Geophys. Res. Lett.* **13**, 173–176 (1986).
5. Jimenez, E., Cara, M. & Rouland, D. *Bull. seism. Soc. Am.* (in the press).
6. Romanowicz, B., Cara, M., Fels, J. F. & Rouland, D. *Eos* **65**, 753–754 (1984).
7. Romanowicz, B. & Monfret, T. *Ann. Geophysicae* **4** (B3), 271–283 (1986).
8. Jackson, J. & McKenzie, D. P. *Geophys. J. R. astr. Soc.* **93**, 185–264 (1984).
9. Ouyed, M. *et al. Nature* **292**, 26–31 (1981).
10. Berberian, M. *Bull. seism. Soc. Am.* **69**, 1861–1887 (1979).
11. Gorshkov, G. P. *Regionalnaya Seismotektonika Territorii Yuga SSR* Izdatelstvo Nauka, Moscow (1984).
12. Zhidkov, M. P., Rotvain, I. M. & Sadovski, A. M. *Vichislitelnaya Seismologia, Moskva, Nauka* **8**, 53–70 (1975).
13. Gvishiani, A. & Kosobokov, V. *Iveztiya Akademiya Nauk, Fizika Zemli* **2**, 21–36 (1981).

ACKNOWLEDGEMENTS. This work was made possible by the cooperation between the French CNRS and the Soviet Academy of Sciences. Financial support for the field operation was provided by the Institut National des Sciences de l'Univers (INSU), the Secrétariat d'Etat aux Risques Naturels Majeurs, the Institut de Physique du Globe de Strasbourg and the Soviet and Armenian Academies of Sciences. The teletransmission system for the Geoscope network is sponsored by INSU. We are deeply indebted to our Armenian colleagues, in particular S. Atchikgueozian, R. Djerbashian and A. S. Karakhanian. The Université de Paris-Sud and the French CEA provided instruments. O. Voevoda, D. Lokshtanov, P. Akelsin, L. Delitsin, I. Parini, A. Romanov, J. Trampert, G. Ball, M. Diament and H. Blumentritt participated in field work. We are indebted to D. Rouland, M. Frogneux, J. M. Holl, J. M. Cantin and E. Speisser for software and hardware.

Phosphorylation of RNA polymerase by the murine homologue of the cell-cycle control protein cdc2

Lars J. Cisek & Jeffry L. Corden*

Howard Hughes Medical Institute and Department of Molecular Biology and Genetics, Johns Hopkins School of Medicine, Baltimore, Maryland 21205, USA

Actively transcribing eukaryotic RNA polymerase II is highly phosphorylated on its repetitive carboxyl-terminal domain. We have isolated a protein kinase that phosphorylates serine residues in this repetitive domain. A component of this kinase is cdc2, the product of a cell-cycle control gene previously shown to be a component of M-phase-promoting factor and M-phase-specific histone H1 kinase. This observation suggests a role for the cdc2 protein kinase in transcriptional regulation.

THE largest subunit of eukaryotic RNA polymerase II (RNAP II) contains an unusual carboxyl-terminal domain (CTD) comprising multiple repeats of the consensus sequence Tyr-Ser-Pro-Thr-Ser-Pro-Ser. This domain is not found in other classes of eukaryotic RNA polymerases or in prokaryotic RNA polymerases. The heptapeptide sequence is repeated, with some degeneracy, 52 times in mouse[1] and Chinese hamster[2], 42–44 times in *Drosophila*[2,3] and 26–27 times in yeast[4,5]. Deletion mutations that result in the loss of more than half of the repeats in mouse and yeast are lethal, indicating that this domain plays an essential role in RNAP II function *in vivo*[2,5,6]. Although the nature of this essential function is unknown, actively transcribing RNAP II is known to be highly phosphorylated on the CTD[7,8].

Three forms of RNAP II (IIO, IIA and IIB) have been described each differing in the apparent relative molecular mass (M_r) of the largest subunit: IIo, 240,000 (240K); IIa, 215K and IIb, 180K. Several lines of evidence have shown that the subunit IIb is derived from the subunit IIa through proteolysis of the CTD[1,9,10]. RNAP II purified by standard techniques consists mainly of forms IIA and IIB; however, if immunoblots of proteins from lysed nuclei are probed with antibodies against the largest subunit, the predominant form is IIo (refs 11, 12). Furthermore, photoaffinity-labelling of actively transcribing RNAP II in *in vitro* extracts or in nuclei reveals primarily subunit IIo, indicating that IIO is the most transcriptionally active form of the enzyme *in vitro* and *in vivo*[7,8].

In vivo labelling studies have shown that the IIo form of the RNAP II largest subunit is highly phosphorylated[13]. Subunit IIo can be converted to IIa by phosphatase treatment, indicating that the higher M_r of IIo is a result of phosphorylation[8]. Analysis of a cyanogen bromide fragment containing the CTD has shown that this domain is multiply phosphorylated on both serine and threonine residues[8]. Thus, IIo appears to be derived from IIa by phosphorylation of the CTD. To understand the role of CTD phosphorylation in RNAP II transcription, we initiated a search for protein kinases that phosphorylate this domain. We report here the isolation of a CTD kinase from mouse ascites tumour cells and demonstrate that the mouse cdc2 protein is a component of this enzyme.

Development of a CTD kinase assay

The CTD is comprised almost entirely of tandem heptapeptide repeats with the consensus sequence Tyr-Ser-Pro-Thr-Ser-Pro-Ser. Reasoning that one or a few of the heptapeptide repeats would, in isolation, adopt a structure similar to heptapeptides within the CTD, we decided to use chemically synthesized heptapeptides as potential protein kinase substrates. The

* To whom correspondence should be addressed.